Interplay between magnetic anisotropy and dipolar interaction in one-dimensional nanomagnets: Optimized magnetocaloric effect

D. Serantes,[1,2,*] V. Vega,[1] W. O. Rosa,[1,3] V. M. Prida,[1] B. Hernando,[1] M. Pereiro,[2] and D. Baldomir[2]

[1]*Departamento de Física, Facultad de Ciencias, Universidad de Oviedo, Calvo Sotelo s/n, 33007 Oviedo, Spain*

[2]*Departamento de Física Aplicada and Instituto de Investigacións Tecnolóxicas, Universidade de Santiago de Compostela, Campus Vida s/n, E-15782 Santiago de Compostela, Spain*

[3]*Centro Brasileiro de Pesquisas Físicas, Rua Dr. Xavier Sigaud, 150, Urca, 22290-180 Rio de Janeiro RJ, Brazil*

(Received 1 March 2012; revised manuscript received 17 May 2012; published 26 September 2012)

The magnetocaloric effect (MCE) in one-dimensional (1D) magnetic nanostructures is optimized for a specific value of the magnetic field H^* when applied perpendicularly to the longitudinal direction of the system. Our results reveal that H^* corresponds to the saturation field, slightly above the transition from a magnetically stable dipolar-coupled configuration to an unstable one. This MCE-optimizing field explicitly depends on the characteristic magnetic parameters of the system, namely, saturation magnetization (M_S) and anisotropy constant (K): H^* is directly proportional to M_S^2, and the anisotropy contribution is equal to the anisotropy field of the particles $H_A = 2K/M_S$. Accordingly, the MCE in 1D nanomagnets can be directly tuned by a proper choice of the characteristic M_S and K values of the materials.

DOI: 10.1103/PhysRevB.86.104431 PACS number(s): 75.75.−c, 75.30.Sg, 75.30.Gw

I. INTRODUCTION

One-dimensional (1D) magnetic nanostructures, such as nanowires and nanoparticle chains, constitute nowadays a very active research field based on their promising use for several nanotechnological applications such as magnetic cellular automata,[1] domain-wall racetrack memory,[2] biomedicine,[3] or plasmon waveguides.[4] In addition, the enhanced anisotropy characteristic of these nanostructures, originated by the magnetic dipolar interaction due to their elongated shape, provides as well a rich theoretical frame for studying the role played by the magnetic anisotropy and dipolar interaction energies on their magnetic response. On this basis, much research effort has been devoted to unveil the magnetic properties of 1D nanomagnetic systems, embracing work ranging from the experimental applied perspective[5] to the purely theoretical modeling.[6]

A central task to address in the characterization of 1D nanomagnetic systems is the role played by the magnetostatic dipolar interaction, and particularly its interplay with the magnetic anisotropy. For implementing nanomagnetic logic devices, it becomes crucial to weight the relative dipolar-coupling influence among nanomagnets;[1] and in regular arrays of magnetic nanowires, the dipolar coupling among wires has been recently shown to be at the origin of a memory effect.[7] It is well known that the magnetostatic dipolar interaction favors the longitudinal alignment of the magnetization for chains of magnetic nanoparticles with collinear easy axes, but misaligned easy axes can erase such ordering and break the dipolar-induced enhanced anisotropy.[8,9] Furthermore, although the main contribution of the magnetic anisotropy is usually along the longitudinal axes of the magnetic nanowires,[10] it may shift to the perpendicular direction depending on the geometry of the samples (packing factor and aspect ratio).[11] Finally, it is worth to emphasize here that also the characteristic parameters of the system (saturation magnetization M_S and magnetic anisotropy K) play a significant role on the magnetic behavior of these nanosystems.[12]

The rich magnetic response of 1D nanomagnets is receiving an increasing attention in the context of the promising *magnetic refrigeration*, a clean and efficient refrigeration technology with high potentiality to substitute the pollutant and inefficient vapor-gas compressing refrigerators currently used.[13] Magnetic refrigeration is based on the *magnetocaloric effect* (MCE), the temperature change ΔT_{ad} undergone by a magnetic material when subjected to the adiabatic variation of a magnetic field.[14] One of the main drawbacks of the magnetic refrigeration is the high economic cost of the materials with largest coolant effect, what hampers its commercialization, and consequently much research effort is being devoted to finding inexpensive MCE materials able to work around room temperature.[15] In the search of the most adequate MCE parameters, not only the type of material, but also the finding of the most appropriate geometrical and implementation conditions are key points to address, i.e., applied field strength,[16] geometry of the magnetic system for desired applications,[17] engineering implementation of the refrigeration cycle,[18] etc. In this regard, a growing attention is being paid to highly anisotropic magnetic nanostructures, which present the benefits of easily tuning the MCE with the magnetic field, and present also the advantages of having a large surface ratio with respect to the bulk counterpart that favors the heat removal, and suitability to be used in complex nanosized gadgets.[19–21] Highly anisotropic systems such as nanowires or chains are excellent candidates fulfilling these requirements.

In this work, we get a deeper insight into the interplay between magnetic anisotropy and dipolar interactions on 1D nanomagnetic systems. Our starting point is the study of a peculiar phenomenon reported in a previous work: the existence of a particular magnetic field value H^* that optimizes the MCE when applied perpendicularly to chains of magnetic nanoparticles with collinear-aligned anisotropy axes.[19] Such optimizing MCE peculiarity has been also found in randomly dispersed nanoparticle systems that interact via dipolar coupling,[22] but a fundamental explanation about its origin still needs to be provided. It is well known that the MCE usually peaks near the Curie temperature T_C at the second-order magnetic phase transition.[23] However, our computational 1D nanomagnetic system does not include atomic exchange

coupling and hence the optimized MCE must have a different origin, presumably of dipolar type.[8] The open question is, therefore, as to how the magnetostatic dipolar coupling can originate such optimizing MCE feature in 1D nanomagnetic systems.

This intriguing result will be the driving force on our study of the complex interplay between magnetic anisotropy and dipolar energies as governing the magnetic response of 1D nanomagnetic systems. For such purpose, we have used a Monte Carlo (MC) technique, which constitutes an insightful tool in order to have a well-defined and perfectly controlled system for computing the magnetic properties of parallel chains of magnetic nanoparticles with collinear aligned easy magnetization axes. Also, we have complemented and compared our MC simulations with experimental data obtained from ordered FeNi nanowire arrays. It is important to note that both systems, magnetic nanowires and chains of magnetic nanoparticles with easy anisotropy axes aligned along the chains, behave in a very similar way in their magnetic response to an external magnetic field perpendicularly applied to the long axis (easy axis) of the system.[20]

II. PHYSICAL SYSTEM

We considered chains of magnetic nanoparticles with uniaxial anisotropy axes collinear along the chain. The chains are regularly arranged parallel to each other, and we considered both a square lattice and a hexagonal one. Figure 1 illustrates the arrangement of 10×10 chains in the square net, each chain made up of 10 particles length. The aspect ratio between center to center of neighboring particles in the same chain (d), and in nearest chains (D) is $d/D = 1/3$.

The particles are assumed to be all equal (shape, size, M_S, K, etc.) for the sake of simplicity, spherical, and single domain with coherent rotation of the inner atomic magnetic moments. The magnetic moment of the particles is proportional to their volume V, so that the magnetic moment of an i particle is given by $|\vec{\mu}_i| = M_S V_i$. The energies governing the magnetic behavior of the system are uniaxial anisotropy (E_A), Zeeman (E_Z), and dipolar (E_D) ones. Thus, the energy per particle for an N-particle system is given by

$$E^{(i)} = -KV_i \left(\frac{\vec{\mu}_i \cdot \hat{n}_i}{|\vec{\mu}_i|} \right)^2 - \vec{\mu}_i \cdot \vec{H} + \sum_{j \neq i}^{N} \left(\frac{\vec{\mu}_i \cdot \vec{\mu}_j}{r_{ij}^3} - 3 \frac{(\vec{\mu}_i \cdot \vec{r}_{ij})(\vec{\mu}_j \cdot \vec{r}_{ij})}{r_{ij}^5} \right), \quad (1)$$

where the energy terms are E_A, E_Z, and E_D, respectively. $\hat{n}_i$ indicates the orientation of the magnetic moment $\vec{\mu}_i$, and $\vec{r}_{ij}$ is the vector connecting particles i and j.

To carry out the simulations of the dependence of the system magnetization ($\vec{M}$) on the applied magnetic field ($\vec{H}$) and on the temperature (T), we have used a MC technique based on the METROPOLIS algorithm, in the same way as in Ref. 19. To drive the orientation of the magnetic moments of the individual particles, we randomly select one and generate (also at random) a new orientation of its magnetic moment, near the original orientation direction.[24] This new position is accepted with probability $\min[1, \exp(-\Delta E/k_B T)]$, where ΔE is the energy difference between trial and old orientations and k_B is the Boltzmann constant. The basic MC *computational time* unit, one MC step, is defined as N attempts to change the magnetic configuration of the system, being $N = 1000$ the amount of magnetic entities (magnetic moments) considered in our simulations. As usual, we use normalized units for the magnetization, magnetic field, and temperature, which are, respectively, given as $m = M/M_S$, $h = H/H_A$, and $t = k_B T/2KV$, being $H_A = 2K/M_S$ the anisotropy field of the particles. The advantage of using normalized units is that the results obtained are valid for any properties of the system under the above requirements. Small differences in the computational procedure (such as periodic/nonperiodic boundary conditions) will be properly described where being necessary.

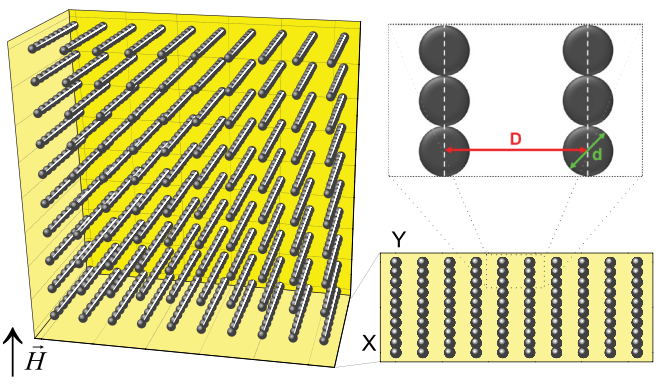

FIG. 1. (Color online) Schematic drawing of the $10 \times 10 \times 10$ square-lattice sample (main panel). Small panels show the projection view YX plane, and the zoom illustrates the interparticle distances between neighboring particles in the same chain (d) and nearest chain (D).

III. OPTIMIZED MAGNETOCALORIC EFFECT

The MCE is usually reported in terms of the *isothermal magnetic entropy change* ΔS_M, easier to obtain from indirect measurements than ΔT_{ad} and estimated as

$$\Delta S_M(T, \Delta H) = \int_{H_i}^{H_f} \left(\frac{\partial M(T,H)}{\partial T} \right)_H dH, \quad (2)$$

where M is the projection of the magnetization of the system along the magnetic field direction and ΔH is the difference between initial and final magnetic field values H_i and H_f, respectively.

Equation (2) indicates that the larger ΔH and $\partial M(H,T)/\partial T$, the higher ΔS_M and therefore the higher the MCE. However, from the practical point of view, it is important to use relatively small H values able to be generated by permanent magnets (usually below 2 T). Hence, it is very important for applications to find a suitable combination between a relatively low ΔH and the corresponding $\partial M(H,T)/\partial T$ ratio able to optimize ΔS_M. In a previous work, we have found a particular magnetic field H^* that optimizes $\partial M/\partial T$ (and hence the MCE) when it is applied perpendicular to 1D chains of magnetic nanoparticles with collinear-aligned anisotropy easy axes.[19] It is our objective now to analyze the origin of such an optimizing feature, paying special attention to the role played by the magnetostatic dipolar interaction.

A. Geometry dependence of the optimized MCE

Our first step on unveiling the nature of H^* is to study its dependence on the geometry of the array of nanochains, i.e., size of the system and spatial symmetry. Our previous results reported in Ref. 19 are based on a 5×5 chain system distributed on a square lattice. Each chain is composed by 10 particles length, and periodic boundary conditions are used that result in an infinite system in the YZ plane. Now, we consider a much larger system of 10×10 chains in a square lattice (same characteristics of each chain), but without periodic boundary conditions; also, the same system is placed on a hexagonal lattice displaying the same interparticle/interchain distance with a (1/3) aspect ratio. For both systems, we have computed the *zero-field cooling* (ZFC) and *field cooling* (FC) curves for different strengths of the applied field, in order to obtain the $\partial M/\partial T$ data ($\partial m/\partial t$ in normalized units).

The ZFC/FC curves for a normalized value of the magnetic field $h = 1.0$ are displayed on the inset of Fig. 2 for the 10×10 chains system in the square and hexagonal lattices, as well as the corresponding data from Ref. 19. Both ZFC and FC curves exhibit a growing trend at low temperatures until a particular maximum value $t_{\max}$ is reached, and a superparamagnetic-like decay above it. Noteworthy, both curves overlap in the whole temperature range for all field values, even for fields well below the anisotropy field of the particles, whereas usual superparamagnetism (SPM) is characterized by a splitting between ZFC and FC curves below the maximum of the ZFC one for low applied magnetic fields, with a continuous increase of the FC curve while decreasing the temperature. This maximum in the ZFC curve is usually approximated as the so-called blocking temperature (T_B), the temperature threshold below which the particles are in the blocked state and show memory (i.e., irreversibility), and above which the particles orient in a paramagnetic-like fashion and show no memory effects (i.e., reversibility).[25] The distinct features of our system indicate that the peak in the ZFC/FC curves does not correspond to T_B. Instead, it can be rather regarded as an ordering temperature with typical characteristics of a phase transition as time and magnetic field independence (see Refs. 8 and 19 for a detailed discussion). These special features originate on the particular geometrical arrangement of the present case, with the magnetic field applied perpendicularly to the magnetic easy anisotropy axes.

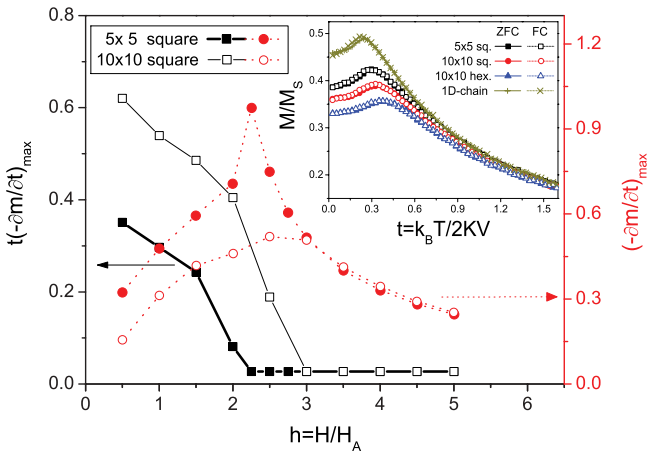

FIG. 2. (Color online) $(-\partial m/\partial t)_{\max}$ (circles) and $t\,(-\partial m/\partial t)_{\max}$ (squares) data vs $h = H/H_A$, for the 10×10 square lattice depicted in Fig. 1 (full symbols), together with the 5×5 square lattice data of Ref. 19 (empty symbols) shown for the comparison. Inset shows the ZFC and FC curves of four different systems (5×5 chains with periodic boundary conditions of Ref. 19; 10×10 finite-size systems both in the hexagonal and square lattice; and a very long single chain of 1000 particles).

The main panel in Fig. 2 shows the maximum of the $-\partial m/\partial t$ data, $(-\partial m/\partial t)_{\max}$, versus the normalized field h for the $10 \times 10 \times 10$ square-lattice case, as well as the temperature dependence of such maximum $t\,(\partial m/\partial t)_{\max}$. These values correspond to the temperature range above the maximum of the curves, where $\partial m/\partial t < 0$ (direct MCE), since the temperature range where $\partial m/\partial t > 0$ (inverse MCE) rapidly disappears with increasing field. A pronounced peak appears at $h^* = 2.25$, very close to the data published in Ref. 19 (reproduced in Fig. 2 for comparison). In fact, it can be noted that the maximum is reached at the same value $h^* = 2.5$ if considering the same precision in the values of h. This coincidence indicates that the existence of the optimizing MCE field is roughly independent of the system size. Furthermore, the results obtained for the hexagonal lattice (not shown) are very similar as well to the square-lattice case, pointing out that the optimizing field h^* appears to be also independent of the spatial distribution of chains and is therefore originated solely by the elongated chainlike geometry with collinear aligned anisotropy.

B. One very long single chain of nanoparticles

In order to confirm the above argument, we have performed similar MC simulations for a particular system that emphasizes the uniaxial and collinear features of the easy anisotropy axes. We consider an isolated very long chain formed by 1000 particles long, so that interactions among neighboring chains are avoided and the broken-symmetry effects at the edges are minimized. The scheme of this very long single chain is illustrated in Fig. 3. The shape and absolute magnitude of the ZFC and FC curves obtained for this isolated chain are very similar to that of the different geometrical arrangements considered (see inset in Fig. 2), indicating that the origin of the optimizing-MCE features lies mainly on the single-chain elongated structure. Interactions among parallel neighboring chains would be second-order effects.

Once we have confirmed that the optimizing MCE arises from the elongated single-chain geometry with collinear easy anisotropy axes, our next step is to perform an exhaustive analysis of the magnetic field dependence of the MCE in such structures. With that aim, we have carried out $m(h)$ simulations, as displayed in Fig. 4(a) for different (normalized) temperatures. The data shown correspond to the positive branch of a full $m(h)$ hysteresis loop for the comparison with the results obtained from the $m(t)$ data plotted in Fig. 2. The computational

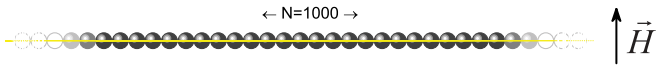

FIG. 3. (Color online) Schematic drawing of a very long single chain with $N = 1000$.

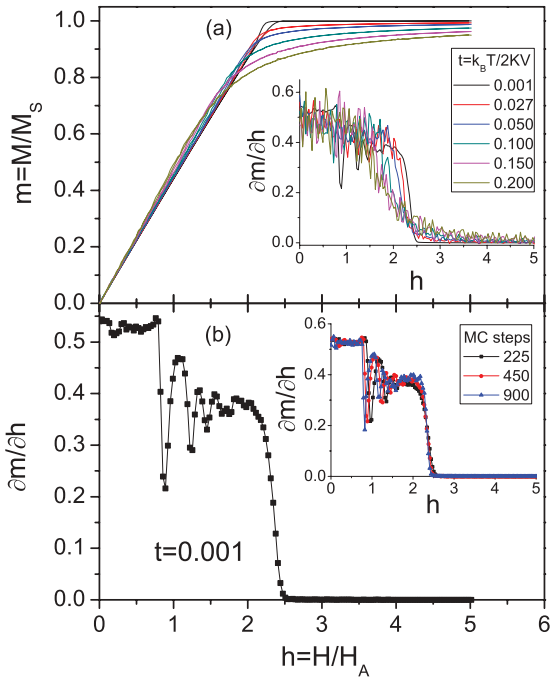

FIG. 4. (Color online) (a) Positive branch of the $m(h)$ hysteresis curves for different normalized temperatures, and (b) the $\partial m/\partial h$ data corresponding to the $t = 0.001$ case. Negative branch is symmetric. Inset in (a) displays the $\partial m/\partial h$ data for different temperatures; inset in (b) illustrates the evolution with larger *computational time* (larger MC steps) of the $\partial m/\partial h$ data corresponding to the $t = 0.001$ case.

procedure was the following: initially, the orientation of the magnetic moments was randomly generated at very high temperature, and then cooled in zero field down to the isothermal temperature of reference. Next, the magnetic field was perpendicularly applied and increased up to $h = 5.0$; then, the field was decreased down to $h = -5.0$, and finally increased again up to $h = 5.0$. The field-variation ratio was $\Delta h = 0.03299$ every 450 MC steps during the entire MC simulation process.[26]

The $m(h)$ data displayed in Fig. 4(a) follow an essentially linear dependence of $m(h)$ until saturation at low temperatures, which progressively smooths with increasing temperature. All curves exhibit a nonhysteretic SPM-like behavior that indicates reversibility, in agreement with the overlapping between the ZFC and FC curves.

More detailed information can be extracted from the corresponding $\partial m/\partial h$ data, as shown in the inset of Fig. 4(a) for the different cases of the main panel. The overall trend of the field derivative of magnetization is a slight decrease with increasing field up to saturation, becoming practically zero for higher-field values. In order to have a more detailed analysis of the $\partial m/\partial h$ data in relation with the optimizing-MCE feature, we focus on the low-temperature-limit case $t = 0.001$ since the optimizing-MCE phenomena occur at low temperatures, as displayed in the main panel of Fig. 4(b). Two remarkable features can be observed in the $\partial m/\partial h$ data: first, an abrupt decay to zero, where the inflection point of the curve indicates the critical field, approximately $h^* = 2.5$. This critical value is straightforward related to the field that optimizes the above-mentioned MCE. Second, and more curious, an oscillating behavior appears for fields roughly above the anisotropy field of the particles ($h = 1$) and below the critical field $h^* = 2.5$. The amplitude of these oscillations attenuates rapidly with increasing h. When the temperature increases, the sharp shapes of both features vanish due to the thermal excitations, as observed in the inset of Fig. 4(a). We have also tested the temporal evolution of these two features, performing the $m(h)$ simulations of the main panel in Fig. 4(b) at different field-variation ratio, $\Delta h = 0.03299$ every 225, 450 (main panel), and 900 MC steps, accounting for diverse *computational time*. The results show that with increasing the computational time, the abrupt change in $\partial m/\partial h$ becomes more accentuated, whereas the oscillations shift to smaller field values [see inset of Fig. 4(b)].

The critical field h^* coincides with the applied field value at which the magnetization of the chain, initially lying along the chain axis and that gradually turns into the perpendicular direction with increasing the external field, reaches the saturation state. At this field h^*, the system undergoes a sudden change in its magnetization state similar to what happens in magnetic phase transitions where also the MCE is enhanced. This analogy could explain why our system shares common optimizing features at the critical field with systems that undergo a second-order (reversible) phase transition. In our case, such change is driven by the strength of the perpendicularly applied magnetic field, whereas in the other case, this phenomenon is usually due to a magnetization dependence on temperature.

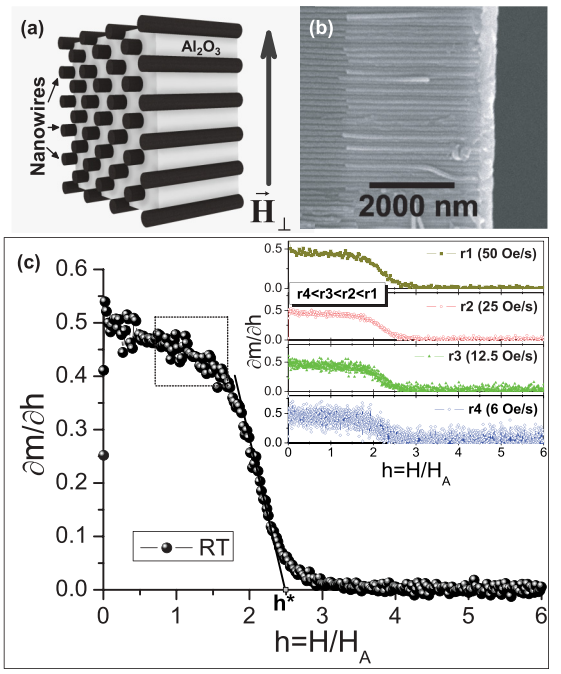

FIG. 5. (Color online) (a) Schematic picture of a highly hexagonally ordered nanowire array in the patterned alumina template; (b) SEM cross-section view of the parallel aligned $Ni_{80}Fe_{20}$ nanowires embedded in the alumina template; and (c) $\partial m/\partial h$ vs h data measured at room temperature (RT), where the dotted square indicates the oscillations observed in $\partial m/\partial h$ at the same field range than in the MC simulations. The solid line indicates how to estimate h^*. Inset in (c) shows $\partial m/\partial h$ vs h data obtained at different field rates of measurement.

C. Comparison with the experimental system

With the purpose of experimentally confirming the (thermo)magnetic behavior predicted by our simulations, we have measured the $M(H)$ loops in spatially ordered $Ni_{80}Fe_{20}$ (Permalloy) nanowires arrays when applying a magnetic field perpendicular to the wires' axis. This comparison is feasible based on the similar magnetic behavior exhibited by ferromagnetic nanowires and chains of magnetic nanoparticles,[20] as it was pointed out in the Introduction.

Magnetic nanowires were fabricated by electrochemical deposition in nanoporous alumina (Al_2O_3) templates, as reported elsewhere.[27] The nanowires are spatially distributed following a hexagonal centered arrangement, with main average diameter around $d = 35$ nm and interwire (center-to-center) distance of $D = 105$ nm, i.e., keeping the same aspect ratio (1/3) as considered in the MC simulations. A schematic drawing of the nanowires' array embedded into the alumina template is shown in Fig. 5(a), and Fig. 5(b) shows a SEM cross-section view of the sample. Since we have already proven that the magnetic response of the system is roughly independent of the spatial arrangement of the 1D chains (Sec. III A), we can directly compare these experimental results with our simulated ones.

In Fig. 5(c), we show the $\partial m/\partial h$ versus h curves. Those curves correspond to the case of the magnetic field applied perpendicular to the nanowires, as depicted in Figs. 5(a) and 5(b), where the normalizing anisotropy field H_A ($\approx$2 kOe) was obtained from the longitudinal $M(H)$ curves measured when applying the magnetic field parallel to the nanowires' axis. It can be appreciated from the main panel of Fig. 5(c) that the field value h^* that optimizes the maximum of the MCE of the system is reached at the extrapolated field value to the h axis going through the inflection point in the $\partial m/\partial h$ curve, which occurs at around $h = 2.5$ (i.e., calculated in a similar way as that of the *Curie temperature* T_C of a magnetic material). This result fits well to those obtained from MC simulations for chains of collinear nanoparticles. The black square indicates the appearance of some oscillating features in the $\partial m/\partial h$ curve that occur near the anisotropy field value, as obtained also in the MC simulations.

The inset of Fig. 5(c) shows the effect of the time of measurement in the $\partial m/\partial h$ versus h curves, taken at four different rates of field measurement, namely, 50 Oe/s, 25 Oe/s, 12.5 Oe/s, and 6 Oe/s, respectively. The main idea is to study the influence of reducing the time interval or average of measurements in order to investigate the magnetic behavior of our system by minimizing its response time interval to the applied field and to search the oscillating features in the derivative of magnetization versus changes in the applied field from saturation down to the remanent state. It can be clearly seen that while the noise in the magnetization derivative increases when reducing the field rate, the optimizing field value h^* does not change in a significant way. Therefore, this experimental system constituted by an ordered array of ferromagnetic nanowires reproduces nearly all the features required for the optimization of its MCE, when a particular field value of h^* is applied perpendicularly to the wires' axis.

IV. DISCUSSION

In Sec. III, we have found that the optimizing-MCE field h^* is originated by the chainlike characteristic of the system, and occurs roughly at saturation of the magnetization. Our purpose now is to discuss the origin of such optimizing feature, which is very close to what happens in phase transitions, from the point

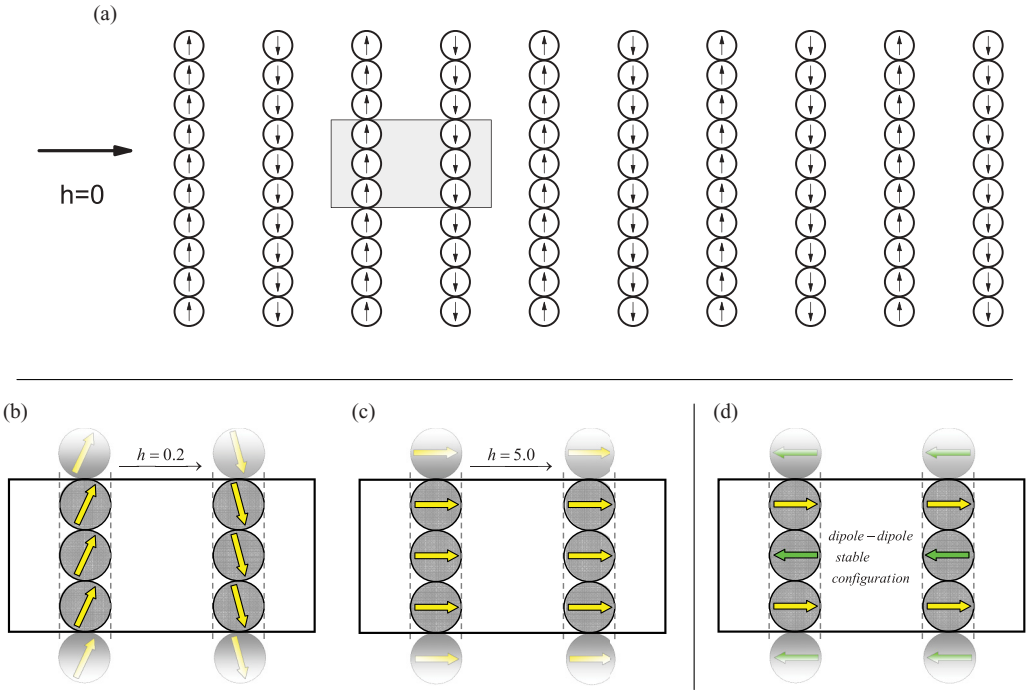

FIG. 6. (Color online) Schematic drawing of the change in the magnetic ordering of some parallel chains under different magnitudes of the perpendicularly applied magnetic field h: (a) $h = 0$, ground-state arrangement of the magnetic moments; (b) small field $h = 0.2$; (c) large field $h = 5.0$; (d) ideal AFM-like dipolarly energetically stable ordering.

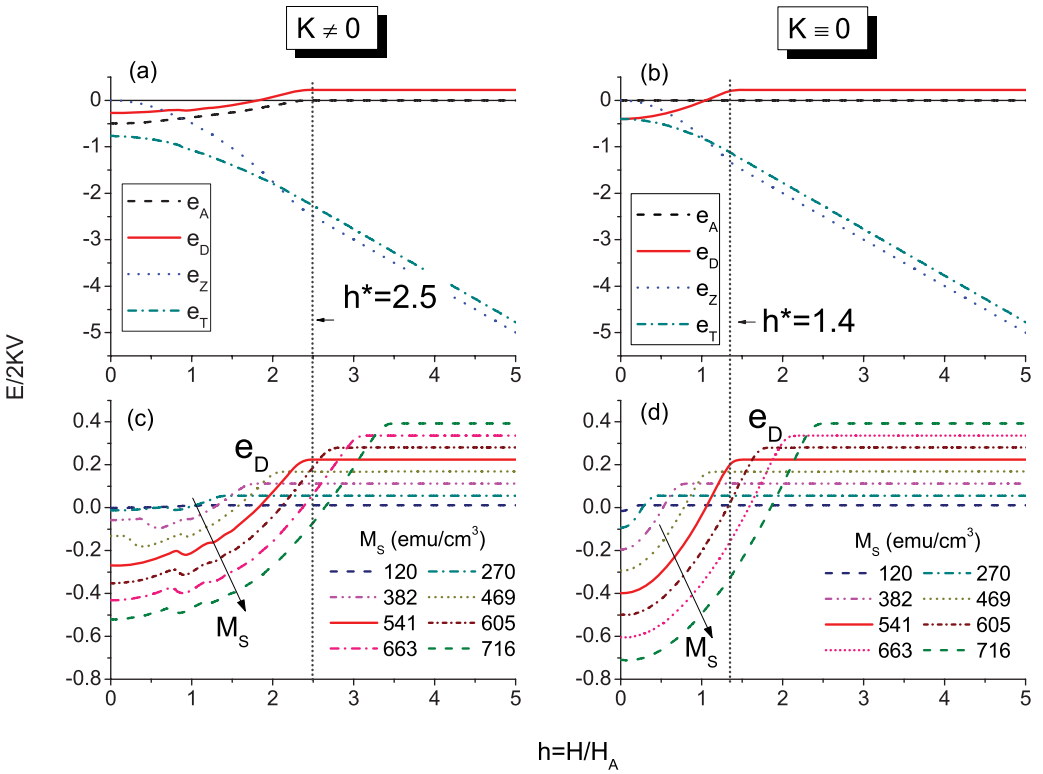

FIG. 7. (Color online) (a) Field dependence of the different energy contributions in normalized units of $E/2$ KV, for the case with anisotropy; (b) same energies as in (a), for the system without anisotropy; evolution of the dipolar energy vs h for different vales of M_S, both for the anisotropy (c) and non-anisotropy cases (d), where the solid (red) curves reproduce the dipolar energy curves of cases (a) and (b), respectively. Vertical dotted lines stand for the corresponding h^* values.

of view of the microscopic magnetic ordering configuration of the system.

Our interpretation of the phenomenon is schematically depicted in Fig. 6 as follows: (a) in the low-field-limit case $h = 0$, the configuration of the magnetic moments inside each chain is of ferromagnetic (FM) type in the longitudinal direction; (b) under a low applied field (low in comparison with H_A, i.e., $h \ll 1$), the magnetic moments gradually deviate from the equilibrium position in the field direction, but still the in-chain FM configuration is energetically stable from the dipolar-coupling energy viewpoint; (c) for a very large field (again, large in comparison with H_A, i.e., $h \gg 1$), the magnetic configuration is FM-like type in the perpendicular direction; (d) whereas the dipolar coupling would rather prefer an out-of-chain antiferromagnetic- (AFM-) like arrangement. We surmise that the optimizing-MCE critical field h^* is the threshold that marks the transition from the low-field dipolarly stable magnetic configuration of case (b), to the unstable arrangement of case (c). Especially relevant is the difference between the field-driven FM-like ordering in the perpendicular direction (c), energetically unstable, and the ideally stable AFM-like arrangement one, as shown in (d). We have used a large system, instead of a single chain, to emphasize that the argument is valid independent of the spatial arrangement of the particles as long as the chainlike configuration is maintained. Interchain interactions may modify the value of the critical field h^*, but do not make disappear the optimizing feature.

To check our interpretation, we have performed a detailed analysis of the different energies governing the magnetic response of the system (namely, Zeeman, anisotropy, and dipolar one), an insightful tool provided through the MC method for studying the underlaying physics. Our interpretation is that if the optimizing-MCE feature originates at the change from a dipolarly stable configuration to an unstable one, this would be directly reflected in the dipolar energy with a change from a negative value to a positive one. The analysis of the energies involved in the $m(h)$ processes is presented in normalized units of energy respect to 2 KV, i.e., $e_A = E_A/2$ KV, $e_D = E_D/2$ KV, and $e_Z = E_Z/2$ KV. Also, the total energy E_T is presented in normalized units $e_T = E_T/2$ KV, with $e_T = e_A + e_D + e_Z$. These normalized units are used with the purpose of making easier the comparison of their relevance with the thermal energy (with the normalized temperature $t = k_B T/2$ KV). In Fig. 7(a), it is shown the evolution of the different energy contributions versus applied field, together with the total one, for the $t = 0.001$ case.

The evolution of the energy contributions displayed in Fig. 7(a) shows that with increasing field, the absolute value of the uniaxial anisotropy energy decreases and eventually reaches zero value, while the dipolar one increases from negative (stable) values until reaching the zero value and then becomes positive, reaching its maximum value at h^*. The dipolar energy changes its sign at a field value slightly smaller than h^*, while h^* coincides with the value at which the anisotropy energy reaches zero (the latter becomes evident

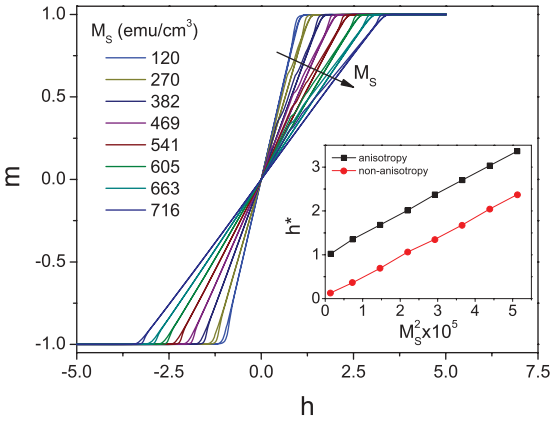

FIG. 8. (Color online) $m(h)$ hysteresis cycles for the case with uniaxial anisotropy, for different M_S values. Inset shows the dependence of the critical field h^* on M_S^2, both for the anisotropy and non-anisotropy cases.

since at saturation the magnetization and uniaxial anisotropy are perpendicular). Therefore, the explanation for the existence of the optimizing field h^* seems to be more related to the vanishing of the anisotropy energy than to the change in the dipolar-coupling configuration. Increasing the value of the applied field makes the magnetic moments to progressively separate from the easy anisotropy axis, resulting in a decrease of the anisotropy energy. Hence, the amount of freedom degrees increases and counterbalances the constraint due to the increasing of the Zeeman energy, thus resulting in an increase of the magnetic entropy. This result is in agreement with previous results reported in the literature, which predict an increase of ΔS_M in systems with decreasing the magnetic anisotropy.[28] Once the uniaxial magnetic anisotropy energy reaches zero, larger field values make to decrease the amount of freedom degrees available and therefore ΔS_M drops. The threshold between both behaviors occurs at h^*.

With the purpose of further investigating this behavior, we have considered the same system but neglected the uniaxial anisotropy, i.e., we considered that the only energies governing the system are the dipolar and Zeeman. This case is shown in Fig. 7(b); note that we conserved the H/H_A units in the field axis with the only purpose of facilitating the comparison with the case with uniaxial anisotropy, but in fact what matters is that they have the same values in real units. In this non-anisotropy case, it is observed that h^* becomes much smaller but is still bigger than the field at which the sign of the dipolar energy changes, i.e., optimizing occurs at saturation. Interestingly, the difference between the critical fields for the anisotropy and non-anisotropy cases seems to be of the order of the anisotropy field of the particles. Therefore, in order to have more information about the interplay between the dipolar and anisotropy energies, we have for both scenarios (anisotropy and non-anisotropy cases) systematically varied the strength of the dipolar interaction by changing the value of M_S.

In Figs. 7(c) and 7(d), we show, respectively, the evolution of the dipolar energy with the applied magnetic field for the system with and without uniaxial anisotropy. The main differences between both cases are that saturation is always reached at smaller field values for the non-anisotropy case, and that oscillations are only observed for the anisotropy case. The absolute values of the dipolar energy at low fields are larger for the non-anisotropy case, reflecting the fact that when the uniaxial anisotropy is present, the chains can be broken[8] and hence the dipolar energy is smaller. As expected, the dipolar energy values at saturation are the same for both cases because they are equivalent when the anisotropy energy reaches zero value for the uniaxial anisotropy case.

The difference between the critical field of the anisotropy and non-anisotropy cases is nearly one in units of the anisotropy field, suggesting that the uniaxial anisotropy adds a contribution to the critical field equivalent to the anisotropy field. In order to check this possibility, we have systematically analyzed the value of h^* for both cases. The results are plotted in Fig. 8. Here, we observe that larger values of M_S require larger fields to magnetically saturate the system, illustrating the stronger dipolar-coupling strength. The inset shows that h^* follows a linear dependence on M_S^2, both for the anisotropy and non-anisotropy cases. Remarkably, the difference between both cases is equivalent to the anisotropy field of the particles.

V. CONCLUSIONS

We have obtained by means of a computational Monte Carlo technique that for chains of magnetic nanoparticles with collinear aligned easy anisotropy axes under a perpendicularly applied magnetic field, it is possible to identify a particular field value h^* that optimizes the MCE. This property is mainly originated by the particular elongated geometry of the system, and is also experimentally observed in ordered arrays of ferromagnetic FeNi nanowires. Its origin lays on a complex interplay between the uniaxial magnetic anisotropy and the dipolar interaction energies, and can be identified as the saturating field. Interestingly, h^* depends linearly on M_S^2, and the anisotropy energy adds a contribution equivalent to the anisotropy field of the particles H_A. Our MC simulation model demonstrates that the dipolar interaction energy remains in the origin of the existence of a critical field H^* for optimizing the MCE.

These results may be very useful for the design of specific MCE applications since the properties of the system can be tuned by the combination of K and M_S. It is important to note that while the MC simulations predict h^* to occur in the low-temperature limit, the experimental measurements indicate, however, that it is possible to observe such an MCE-optimizing feature also at room temperature, more desirable for MCE applications.

In addition, we also reported on the existence of an oscillating feature in the $\partial M/\partial H$ data, slightly above the anisotropy field of the particles and that disappears if no uniaxial anisotropy is considered. Further work is necessary in order to gain deeper understanding on the nature of these oscillations.

ACKNOWLEDGMENTS

We acknowledge the CESGA (Centro de Supercomputación de Galicia) for the computing facilities. The Spanish MICINN is also acknowledged for the financial support through Projects No. MAT2009-13108-C02-01, No.

MAT2010-20798-C05-04, and Xunta de Galicia for Project No. INCITE08PXIB236053PR. D. Serantes thanks FICyT (Contract No. FC-10-COF10-04). W. O. Rosa acknowledges the Brazilian agencies FAPERJ and CAPES for the financial support. The scientific support from the University of Oviedo SCT's is also acknowledged.

*david.serantes@gmail.com

[1] A. Imre, G. Csaba, L. Ji, G. H. Bernstein, and W. Porod, Science **311**, 205 (2006).

[2] S. S. P. Parkin, M. Hayashi, and L. Thomas, Science **320**, 190 (2008).

[3] D. S. Choi, J. Park, S. Kim, D. H. Gracias, M. K. Cho, Y. K. Kim, A. Fung, S. E. Lee, Y. Chen, S. Khanal, S. Baral, and J. H. Kim, J. Nanosci. Nanotechnol. **8**, 2323 (2008).

[4] R. P. Cowburn and M. E. Welland, Science **287**, 1466 (2000).

[5] J. Juarez, A. Cambon, A. Topete, P. Taboada, and V. Mosquera, Chem. Eur. J. **17**, 7366 (2011).

[6] K. Warda, J. Phys.: Condens. Matter **21**, 345301 (2009).

[7] X. Kou, X. Fan, R. K. Dumas, Q. Lu, Y. Zhang, H. Zhu, X. Zhang, K. Liu, and J. Q. Xiao, Adv. Mater. **23**, 1393 (2011).

[8] D. Serantes, D. Baldomir, M. Pereiro, B. Hernando, V. M. Prida, J. L. Sánchez Llamazares, A. Zhukov, M. Ilyn, and J. González, J. Phys. D: Appl. Phys. **42**, 215003 (2009).

[9] A. A. Bukharov, A. S. Ovchinnikov, N. V. Baranov, and K. Inoue, J. Phys.: Condens. Matter **22**, 436003 (2010).

[10] D. A. Allwood, G. Xiong, C. C. Faulkner, D. Atkinson, D. Petit, and R. P. Cowburn, Science **309**, 1688 (2005).

[11] G. Kartopu, O. Yalcin, K. L. Choy, R. Topkaya, S. Kazan, and B. Aktas, J. Appl. Phys. **109**, 033909 (2011).

[12] S. Hariharan and J. Gass, Rev. Adv. Mater. Sci. **10**, 398 (2005).

[13] E. Brück, J. Phys. D: Appl. Phys. **38**, R381 (2005).

[14] V. K. Pecharsky and K. A. Gshneidner, J. Magn. Magn. Mater. **200**, 44 (1999).

[15] K. A. Gshneidner and V. K. Pecharsky, Int. J. Refrig. **31**, 945 (2008).

[16] D. Baldomir, J. Rivas, D. Serantes, M. Pereiro, J. E. Arias, M. C. Buján-Núñez, and C. Vázquez-Vázquez, J. Non-Cryst. Solids **353**, 793 (2007).

[17] B. Hernando, J. L. Sánchez-Llamazares, V. M. Prida, D. Baldomir, D. Serantes, M. Ilyn, and J. González, Appl. Phys. Lett. **94**, 222502 (2009).

[18] R. Bjørk, C. R. H. Bahl, A. Smith, and N. Pryds, Int. J. Refrig. **33**, 437 (2010).

[19] D. Serantes, D. Baldomir, M. Pereiro, B. Hernando, V. M. Prida, J. L. Sánchez Llamazares, A. Zhukov, M. Ilyn, and J. González, Phys. Rev. B **80**, 134421 (2009).

[20] V. M. Prida, V. Vega, D. Serantes, D. Baldomir, M. Ilyn, A. P. Zhukov, J. González, and B. Hernando, Phys. Status Solidi A **206**, 2234 (2009).

[21] V. Franco, K. R. Pirota, V. M. Prida, Antonio Maia J. C. Neto, A. Conde, M. Knobel, B. Hernando, and M. Vázquez, Phys. Rev. B **77**, 104434 (2008).

[22] D. Serantes, D. Baldomir, M. Pereiro, J. Rivas, C. Vázquez-Vázquez, M. C. Buján-Núñez, and J. E. Arias, Phys. Status Solidi A **205**, 1349 (2008).

[23] V. Franco and A. Conde, Int. J. Refrig. **33**, 465 (2010).

[24] For the simulations, in Ref. 19 the trial new orientation of the magnetic moment was randomly generated inside a cone of angle 0.1 radian. In this study, we have included a slight modification of this procedure, consisting on treating the angle as temperature dependent, following the work of U. Nowak *et al.*, Phys. Rev. Lett. **84**, 163 (2000), in the same way as described in D. Serantes *et al.*, J. Appl. Phys. **108**, 073918 (2010). It is worth to mention that this alternative was used because we consider it more realistic (it results in larger oscillations at higher temperatures), but the same features of critical field and oscillations appear if using a constant cone angle of 0.1 radian.

[25] D. Serantes and D. Baldomir, Open Surf. Sci. J. **4**, 71 (2012).

[26] The selected field variation ratio $\Delta h/\Delta \mathrm{MC}$ steps $= 0.03299$ every 450 MC steps, was chosen because of the following reasons: on the one hand, that field-variation ratio is very comparable to real-field variation units, for example, for Ni nanoparticles as those used in Ref. 19, it is equivalent to a 50-Oe field variation. On the other hand, with that amount of MC steps, we reproduced the Stoner-Wohlfarth model, at very low temperature, i.e., $H_C = 0.48 H_A$ and $M_R = 0.50 M_S$ at $t = 0.001$.

[27] V. M. Prida, K. R. Pirota, D. Navas, A. Asenjo, M. Hernández-Vélez, and M. Vázquez, J. Nanosci. Nanotechnol. **7**, 272 (2007).

[28] D. Baldomir, D. Serantes, M. Pereiro, J. Rivas, C. Vázquez-Vázquez, M. C. Buján-Núñez, and J. E. Arias, Phys. Status Solidi A **205**, 1343 (2008).